A New Approach to Moving Targets and Background Separation in Multi-Channel SAR

Di Wu, Mehrdad Yaghoobi and Mike Davies
School of Engineering
University of Edinburgh
UK, EH9 3JL
Email: {D.Wu, m.yaghoobi-vaighan, mike.davies}@ed.ac.uk

***Abstract*—This paper describes a new approach for decoupling the slowly-moving targets and the clutter under multi-channel SAR (Synthetic Aperture Radar) scenarios. Given the phase histories received by different channels, the high-level data structures, e.g. the sparsities of moving targets, enable us to enforce advanced constraints on an optimisation problem to distinguish the dynamic targets from static background. Specifically, an iterative method is employed for the decomposition by alternatively updating the arguments. The dynamic parts can then be used for the subsequent analysis on states of the targets, and the static parts, in the case that the background does not change significantly over time, can be inherited in subsequent sub-aperture processings. The presented approach is demonstrated on simulated three-channel SAR data.**

***Index Terms*—SAR, GMTI, sparsity, compressed sensing**

I. Introduction

Synthetic Aperture Radar (SAR) can be traced back to 1950s when the military was in need of a remote surveillance device with all-weather, day-or-night capability. By superimposing the received signals along the flight path, SAR imaging systems synthesise a large virtual aperture to provide high spatial resolution images. It is well known that moving targets will be displaced and blurred in the formed images. One appealing application for SAR is Ground Moving Target Indicator (GMTI) which aims at revealing the moving targets in the SAR images and correcting their patterns.

Displaced Phase Center Antenna (DPCA) [1] and Along Track Interferometry (ATI) [2] are the widely used subtractive methods in the SAR/GMTI community which expose the moving targets with magnitudes and interference phases respectively. DPCA is noise-limited since the noise can corrupt the differential image between different channels and ATI is clutter-limited since the clutter will contaminate the image phases if its energy is comparable to the moving targets [3]. They are all taken as the practical clutter cancelation algorithms which perform moving targets detections instead of thorough decomposition (though ATI is capable of estimating radial velocities of targets).

In this paper we introduce an optimization based approach with an iterative process to decompose the raw data into two portions which correspond to the moving targets and background respectively. The proposed method is designed to integrate GMTI abilities and give imaging abilities on both moving targets and static clutter. The remainder of this paper is organized as follows. Section two describes the signal modeling of a standard multi-channel SAR system. In section three, the SAR processing basics, and the moving targets and background separation approach are presented. Section four demonstrates the performance of the proposed method with a simulated three-channel SAR scenario. The conclusions are discussed in section five.

II. Signal Modeling

Based on Fig. 1 we depict a multi-channel SAR platform in the spotlight mode with the moving targets in the observed scene. The phase centres of antennas are spatially separated by a distance d (evenly spaced) on the flight path of the platform. Let the azimuth time of the transmitted pulses be τ_n where $n = \{1, 2, ..., N\}$ is the pulse number; $\mathbf{r}(\tau_n)$ denotes the position of one target at τ_n; $r_i^{(t)}(\tau_n)$ and $r_i^{(o)}(\tau_n)$ represent the distance from the target to the $i-$th antenna and the distance from the scene origin to the corresponding antenna position. The platform velocity within a short sub-aperture can also be approximated with a constant v_p.

The discrete received signals for a target after the dechirping process (the platform motion is compensated with reference to the scene origin) are given by:

$$Y_i(f_k, \tau_n) = A_i \sigma(\mathbf{r}(\tau_n)) \exp\left(-\frac{j4\pi f_k u_i(\tau_n)}{c}\right) \qquad (1)$$

where $\{f_k | k = 1, 2, ..., K\}$ denotes the range frequencies; A_i is a nominal factor for the $i-$th channel which accounts for the beam pattern and energy loss; $\sigma(\mathbf{r}(\tau_n))$ represents the complex reflectivity of the moving target at the location $\mathbf{r}(\tau_n)$; c is the speed of light and $u_i(\tau_n)$ denotes the differential range $r_i^{(t)}(\tau_n) - r_i^{(o)}(\tau_n)$. Given the collection of the target reflectivities $\mathbf{X} \in \mathbb{C}^{M \times L}$, we have the received signals in matrix-vector form as $\mathbf{Y}_i = \Phi_F(\mathbf{X})$ where Φ_F is the forward projection operator projecting from the image domain to data domain.

III. Moving Targets and Background Decomposition

A. SAR Pre-processing

In SAR/GMTI, the raw data is first pre-processed with channel balancing techniques [4] to retrieve the same responses for stationary targets between different channels. We denote

978-1-5090-0863-6/16/$31.00 ©2016 IEEE

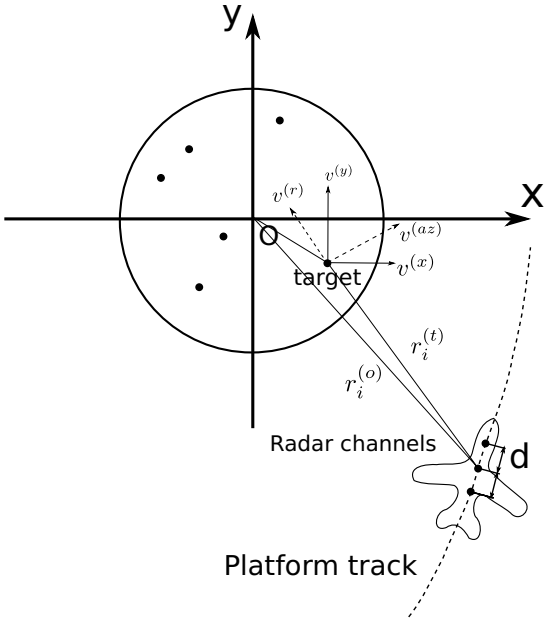

Fig. 1. The geometry of a multi-channel SAR system with moving targets in the monitored scene.

$\widetilde{\mathbf{Y}}_i = \{\widetilde{Y}_i(f_k, \tau_n)\} \in \mathbb{C}^{K\times N}$ as the balanced data for the $i-$th channel. Suppose the radar channels share the same track, the received echo of the aft-antenna can be viewed as the delayed received signal of the fore-antenna, if the monitored scene does not change over time. In the case that the transfer functions of different channels have been equalised, we have that $\widetilde{Y}_i(f_k, \tau_n) = Y_i(f_k, \tau_n + (i-1)\Delta)$ where $\Delta = d/v_p$.

B. SAR Imaging

The typical SAR imaging mechanism, based on widely accepted assumptions of static scene and isotropic reflectors, is modeled as the following linear inverse problem $\mathbf{Y} = \Phi_F^0(\mathbf{X}) + \mathbf{e}$, where $\mathbf{Y}$ is the phase history, $\mathbf{X}$ is the formed image, $\mathbf{e}$ stands for the noise and Φ_F^0 is the forward projection operator assuming stationary scene. The SAR image formation is equivalent to finding the solution of an optimisation problem:

$$\min_{\mathbf{X}} \|\mathbf{Y} - \Phi_F^0(\mathbf{X})\|_F^2 \tag{2}$$

where $\|\|_F$ represents the Frobenius norm. A number of algorithms have been proposed to solve this model. One widely used solution is $\mathbf{X} = \Phi_B^0(\mathbf{Y})$ which employs the backward projection operator Φ_B^0 to approximate the pseudo inverse of Φ_F^0 with its Hermitian transpose.

C. Moving Targets and Background Separation

There have been investigations on the exploitation of sparsity in SAR moving target imaging and detection [5][6][7]. Motivated by practical SAR/GMTI methods and SAR imaging models, the features of the moving targets, which are exploited by DPCA and ATI, can be used to constrain the SAR image forming optimisation. In combination with other high level data structures, such as sparsity, the SAR/GMTI scenarios can be better described with a hybrid DPCA/ATI type model [8] from the mathematical perspective. Efficiently solving the enriched model has opportunities to realise versatile utilities in SAR/GMTI and establish thorough understandings over the data flow.

Given that the de-chirped and channel balanced phase history for channel i is $\widetilde{\mathbf{Y}}_i$ (here the antennas are assumed equally spaced), we apply variable splitting to the image domain, and respectively denote $\mathbf{X} \in \mathbb{C}^{M\times L}$ and $\mathbf{F} \in \mathbb{C}^{M\times L}$ (displaced and defocused) as the stationary background and moving target reflectivities in the first channel. It is then reasonable to assume that $\mathbf{F}$ is sparse compared to the whole scene. It is also well known that the formed image of one moving target will have a phase difference $(4\pi/c)f_0 v_r(d/v_p)$ between two channels, in which f_0 stands for the central frequency of the transmitted signal, v_r is the radial velocity of the target, d denotes the spatial gap between the two channels. This phase shift is a function of v_r and assumed to be constant for one target within a short sub-aperture. The following model is then introduced to decouple the moving targets and stationary clutter:

$$\begin{aligned} \min_{\mathbf{X},\mathbf{F},\mathbf{P}} \quad & \frac{1}{2}\sum_i \|\widetilde{\mathbf{Y}}_i - \Phi_F^0(\mathbf{X} + \mathbf{F}\odot\mathbf{P}^{(i-1)})\|_F^2 \\ s.t. \quad & \mathbf{X} \in \mathbb{C}^{M\times L}, \mathbf{F} \in \mathbb{C}^{M\times L}, \mathbf{P} \in \mathbb{C}^{M\times L} \\ & \|\mathbf{F}\|_0 \le s \\ & |\mathbf{P}_{ml}| = 1,\ m = 1,\dots,M,\ l = 1,\dots,L \\ & \mathrm{supp}(\mathbf{F}) = \mathrm{supp}(\mathbf{P\text{-}1}) \end{aligned} \tag{3}$$

where $\mathbf{P}$ is a pure phase correction matrix which is element-wise magnitude 1 ($\mathbf{P}_{ml} = \exp(j0) = 1$ for static object (m,l) with 0 phase shift), $\odot$ is the element-wise product operator, s stands for the sparsity constraint of the moving target reflectivities. $\mathbf{F}$ and $\mathbf{P\text{-}1}$ are expected to be non-zero only on the moving targets pixels and share the same support. Presumably since the antennas are assumed to be equally spaced, $\mathbf{P}^{(i)}$ is defined as:

$$\mathbf{P}^{(i)} = \underbrace{\mathbf{P}\odot\ldots\odot\mathbf{P}}_{\mathrm{i}} \tag{4}$$

where $i > 0$ and $\mathbf{P}^{(0)} = \mathbf{1}$.

The minimization model (3) is interpreted as forming the SAR images for the moving targets $\mathbf{F}$ and static background $\mathbf{X}$, and estimating the phase corrections $\mathbf{P}$, based on optimising the data consistencies upon the received data sets and enforcing the sparsities and phase shifts on the moving targets. Also we expect to see better matches between the phase histories and forwarded SAR images compared to conventional imaging techniques, and the estimated $\mathbf{X}$ can be naturally used for other sub-aperture processings.

Since directly solving (3) is challenging, we hereby employ an iterative process for practical uses. The variables $\mathbf{X}$, $\mathbf{F}$ and $\mathbf{P}$ can be estimated alternatively by fixing others and updating one variable each time. The estimations of $\mathbf{F}$ and $\mathbf{P}$ are not straightforward, we thus reformulate (3) and introduce

intermediate variables. Let $\mathbf{dX}^i = \mathbf{F} \odot \mathbf{P}^{(i)} - \mathbf{F} \odot \mathbf{P}^{(i-1)}$ and $\mathbf{X}_1 = \mathbf{X} + \mathbf{F}$. Then for I channels we have:

$$\begin{aligned} &\min_{\mathbf{X}_1, \mathbf{dX}_i} \frac{1}{2}\|\widetilde{\mathbf{Y}}_1 - \Phi_F^0(\mathbf{X}_1)\|_F^2 + \\ &\frac{1}{2}\sum_{i=2}^{I}\|\widetilde{\mathbf{Y}}_i - \Phi_F^0(\mathbf{X}_1 + \sum_{j=1}^{i-1}\mathbf{dX}^j)\|_F^2 \\ &s.t. \quad \mathbf{X}_1 \in \mathbb{C}^{M\times L}, \mathbf{dX}^i \in \mathbb{C}^{M\times L} \\ &\qquad \|\mathbf{dX}^i\|_0 \le \widetilde{s},\ i = 1, \dots, I-1 \end{aligned} \tag{5}$$

The $\mathbf{dX}^i$ $(i = 1, \dots, I-1)$, $\mathbf{F}$ and $\mathbf{P} - \mathbf{1}$ are supposed to have the same support, therefore we can enforce the sparsity constraint on $\mathbf{dX}^i$ in (5).

In each iteration we first update $\mathbf{X}_1$ along the inverse gradient direction. The $\mathbf{dX}^i$ can then be updated with the gradient decent method and hard thresholding operations [9]. The next step is to estimate $\mathbf{P}$ and $\mathbf{F}$ based on the intermediate variables $\mathbf{dX}^i$. To mitigate the expensive computational cost of evaluating the gradients, based on the definitions of $\mathbf{X}_1$ and $\mathbf{dX}^i$, we simply approximate $\mathbf{P}$ and $\mathbf{F}$ with

$$\mathbf{P}_{ml} = \begin{cases} \mathcal{H}_z\left(\mathcal{N}\left(\frac{1}{I-2}\sum_{i=2}^{I-1}\mathbf{dX}^i_{ml} \oslash \mathbf{dX}^{i-1}_{ml}\right)\right) & (m,l) \in \Omega \\ 1 & \text{otherwise} \end{cases} \tag{6}$$

$$\mathbf{F}_{ml} = \begin{cases} \frac{1}{I-1}\sum_{i=1}^{I-1}\mathbf{dX}^i_{ml} \oslash (\mathbf{P}^{(i)}_{ml} - \mathbf{P}^{(i-1)}_{ml}) & \mathbf{P}_{ml} \neq 1 \\ 0 & \text{otherwise} \end{cases} \tag{7}$$

where $\mathcal{H}_z$ is the threshold operator that sets all the small phase shifts, i.e. $|\mathbf{P}_{ml} - 1| < z$ ($z = 0.02$ is a good choice), to zero ($\mathbf{P}_{ml} = 1$) to prevent from having too large $\mathbf{F}_{ml}$, $\oslash$ is the element-wise division operator, $\mathcal{N}$ is the normalisation operator ($\mathcal{N}(\mathbf{P}) = \mathbf{P} \oslash |\mathbf{P}|$) to eliminate the amplitudes of $\mathbf{P}$ and make it a pure phase correction matrix, and Ω is the intersection of the support sets of $\mathbf{dX}^i$ $(i = 1, \dots, I-1)$.

The detailed implementations are specified in Algorithm 1. Particularly μ is the approximated Lipschitz constant for the gradient of function $f(\mathbf{X}) = 1/2\|\widetilde{\mathbf{Y}}_1 - \Phi_F^0(\mathbf{X})\|_F^2$. The $\mathcal{T}(\mathbf{a}, b)$ denotes the hard-thresholding that all the elements in $\mathbf{a}$ which are below b (in magnitudes) are replaced with zeros.

Algorithm 1 : Iterative algorithm for approximating the solution of (3).

Initialisation: $\mathbf{X} \leftarrow \mu\Phi_B^0(\widetilde{\mathbf{Y}}_1)$; $\mathbf{P} \leftarrow \mathbf{1}$; $\mathbf{F} \leftarrow \mathbf{0}$; $\mathbf{dX}^i \leftarrow \mu\Phi_B^0(\widetilde{\mathbf{Y}}_{i+1} - \widetilde{\mathbf{Y}}_i)$ $(i = 1, \dots, I-1)$; $\mathbf{X}_1 \leftarrow \mathbf{X} + \mathbf{F}$; $i \leftarrow 1$; $k \leftarrow 1$
while $k < K$ **do**
  $\mathbf{X}_1 \leftarrow \mathbf{X}_1 - \mu\frac{1}{I}\times$
  $\Phi_B^0\left(\Phi_F^0\left(I\mathbf{X}_1 + \sum_{i=1}^{I-1}(i \times \mathbf{dX}^{I-i})\right) - \sum_{i=1}^{I}\widetilde{\mathbf{Y}}_i\right)$
  while $i < I$ **do**
    $\mathbf{dX}^i \leftarrow \mathbf{dX}^i -$
    $\mu \times \Phi_B^0\left(\Phi_F^0\left(\mathbf{X}_1 + \sum_{j=1}^{i}\mathbf{dX}^j\right) - \widetilde{\mathbf{Y}}_{i+1}\right)$
    $\mathbf{dX}^i \leftarrow \mathcal{T}\left(\mathbf{dX}^i, 1\% \times \|\mathbf{dX}^i\|_F^2\right)$
    $i \leftarrow i + 1$
  end while
  $\mathbf{P}$ from (6)
  $\mathbf{F}$ from (7)
  $\mathbf{dX}^i \leftarrow \mathbf{F} \odot \mathbf{P}^{(i)} - \mathbf{F} \odot \mathbf{P}^{(i-1)}$; $\mathbf{X} \leftarrow \mathbf{X}_1 - \mathbf{F}$
  $k \leftarrow k + 1$
end while

IV. EXPERIMENTAL RESULTS

In this section we consider a simulated scenario to demonstrate the effectiveness of the proposed approach. Within standard Cartesian coordinates, the platform carries a three-channel SAR system in spotlight mode, and the first antenna (fore-antenna) linearly moves from (7000, -25, 7000) m to (7000, 25, 7000) m with velocity $v_p = 200$ m/s. The channels are evenly spaced on the platform track with 0.1 m. The pulse repetition frequency (PRF) is 2000 Hz, the central frequency of the transmitted signal is 10 GHz to simulate an X-band Radar, and the range frequency step size is 800 kHz. The monitored region consists of two moving targets which move from (0, 0, 0) m with (2, 26, 0) m/s and from (-50, 50, 0) m with (-3, -16 , 0) m/s respectively.

We have obtained the phase histories as 313×500 matrices, and the discrete grid to be considered here is 512×512 which corresponds to -100 m$\sim$100 m in x direction and -100 m$\sim$100 m in y direction. Static targets are distributed on this grid and one stronger static target is located at (50, 0, 0) m. ATI is well known to be hampered by the scenarios where moving targets and clutter are mixed together. Relatively stronger amplitudes and random phases are given to the static clutter in a rectangular region on purpose to be mixed with one moving target in the image domain and test the performance of the decomposition. Also we add approximately 16.5 dB Gaussian random noises to the raw data. In the remainder of the paper, we apply the fast back-projection and re-projection algorithms (decimation-in-image) [10] as the backward Φ_B^0 and forward Φ_F^0 operators. The simulated scenario can be found in Fig. 2. It can be seen that the moving target at (0, 0, 0) m is shifted to the top and mixed with the rectangle, the other moving target at (-50, 50, 0) m is shifted to the bottom, and both of them have been majorly defocused along the azimuth direction.

We first fix the three raw phase histories with simple multiplications in the Fourier domain to realise the delay in time domain and complete the channel balancing. Then the three balanced data sets $\widetilde{\mathbf{Y}}_1$, $\widetilde{\mathbf{Y}}_2$ and $\widetilde{\mathbf{Y}}_3$ are processed with the presented moving targets and background decomposition algorithm. Since SAR applications are essentially high volume data processings, as shown in Algorithm 1, we start with a proper initialisation to make $\mathbf{X}$ the scaled back-projected $\widetilde{\mathbf{Y}}_1$ instead of $\mathbf{0}$ and retrieve better results within few iterations. In practice, there exists a crucial structure for $\mathbf{P}$ where its elements for one specific target are approximately constant (proportional to the radial velocity of the moving target). We currently do not enforce this structure in our model, and the

estimations of $\mathbf{X}$ and $\mathbf{F}$ are limited by the accuracy of the estimated $\mathbf{P}$.

The comparisons of the decompositions with different initialisations are shown in Figure. 3. It can be seen that the two iteration implementation with proper initialisations gives us a good enough performance. Here the rectangle is well separated from the moving target. With conventional methods the whole support of the moving targets will be cropped and the amplitudes and phases will not be accurately estimated. The estimated phase correction matrix $\mathbf{P}$ is transferred to the velocities in x direction via $\mathbf{v}_x = \sqrt{2}(c/(4\pi))\angle P(v_p/(f_0 d))$, where $\angle$ is an operator to extract the phases, and the estimated $\mathbf{v}_x$ is shown in Figure. 4. We take the local mean values of $\mathbf{v}_x$ as the estimations for the target velocities and get -2.89 m/s and 2.17 m/s which are close to the ground truths. Here the standard ATI on the first two channels, i.e. $\angle\mathbf{P} = -\angle(\Phi_B^0(\widetilde{\mathbf{Y}}_1) \odot (\Phi_B^0(\widetilde{\mathbf{Y}}_2))^*)$, gives the velocity estimations as -2.87 m/s and 1.5 m/s (local mean values). The ATI results remain consistent for the -3 m/s target but have deviations for the target which is embracing comparable rectangular clutters.

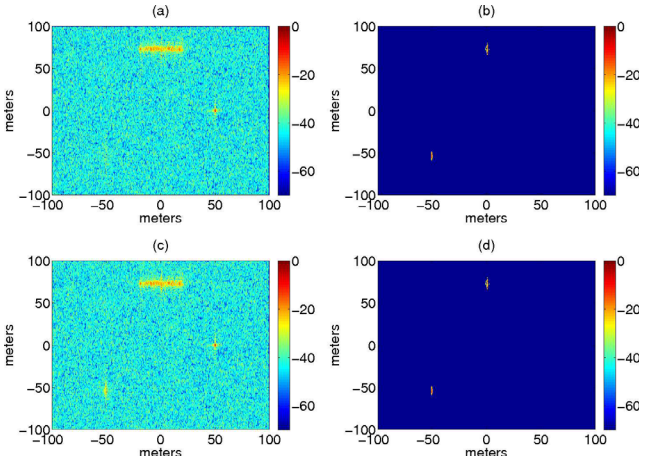

Fig. 3. Decoupled SAR images using the proposed approach. The images here are displayed in dB against the same constant for visual comparisons. (a) The estimated background after 2 iterations with proper initialisations. (b) The estimated moving targets after 2 iterations with proper initialisations. (c) The estimated background after 10 iterations by initialising $\mathbf{X}$ with $\mathbf{0}$. (d) The estimated moving targets after 10 iterations by initialising $\mathbf{X}$ with $\mathbf{0}$.

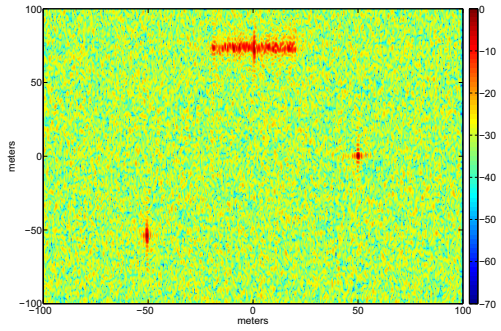

Fig. 2. The formed image in dB based on the first channel data with the fast back-projection algorithm.

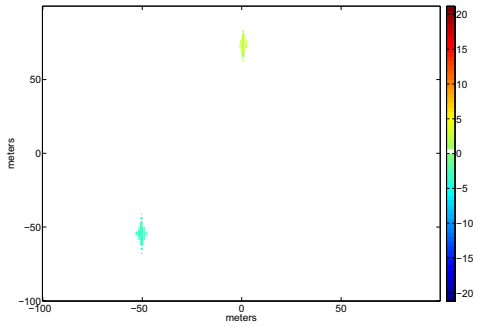

Fig. 4. The estimated velocity map in x direction which correspond to the estimated $\mathbf{P}$ after 2 iterations with proper initialisations.

V. Conclusion

This paper presents a moving target and background separation approach in multi-channel SAR scenarios. Specifically by modeling the phase differences between channels and utilising the sparsities of the moving targets within an optimisation framework, the raw data can be decomposed into dynamic/stationary portions, and the moving/static objects can be imaged. Preliminary results based on an iterative process demonstrate the effectiveness of the proposed approach.

Acknowledgment

This work was supported by the Engineering and Physical Sciences Research Council (EPSRC) grants [EP/K014277/1]; and the University Defence Research Collaboration (UDRC) in Signal Processing.

References

[1] S. Chiu and C. Livingstone, "A comparison of displaced phase centre antenna and along-track interferometry techniques for RADARSAT-2 ground moving target indication," *Canadian Journal of Remote Sensing*, vol. 31, no. 1, pp. 37–51, 2005.

[2] I. Sikaneta and C. Gierull, "Ground moving target detection for along-track interferometric SAR data," in *Aerospace Conference, 2004. Proceedings. 2004 IEEE*, vol. 4, March 2004, pp. 2227–2235 Vol.4.

[3] W. Wang, *Multi-Antenna Synthetic Aperture Radar*. CRC Press, 2013.

[4] C. Gierull, "Digital channel balancing of along-track interferometric SAR data," in *Technical Memorandum DRDC Ottawa TM 2003-024*. Defence R&D, Ottawa, Canada, March 2003.

[5] L. Prunte, "GMTI from multichannel SAR images using compressed sensing," in *Synthetic Aperture Radar, 2012. EUSAR. 9th European Conference on*, April 2012, pp. 199–202.

[6] N. Ozben Onhon and M. Cetin, "Sar moving target imaging using group sparsity," in *Signal Processing Conference (EUSIPCO), 2013 Proceedings of the 21st European*, Sept 2013, pp. 1–5.

[7] D. Wu, M. Yaghoobi, and M. Davies, "Sparsity based ground moving target imaging via multi-channel sar," in *Sensor Signal Processing for Defence (SSPD), 2015*, Sept 2015, pp. 1–5.

[8] R. Deming, M. Best, and S. Farrell, "Simultaneous SAR and GMTI using ATI/DPCA," *Proc. SPIE*, vol. 9093, pp. 90 930U–90 930U–19, 2014.

[9] T. Blumensath and M. E. Davies, "Iterative hard thresholding for compressed sensing," *Applied and Computational Harmonic Analysis*, vol. 27, no. 3, pp. 265 – 274, 2009.

[10] S. Kelly and M. Davies, "A fast decimation-in-image back-projection algorithm for SAR," in *Radar Conference, 2014 IEEE*, May 2014, pp. 1046–1051.